

# The shape and erosion of pebbles

D.J. Durian,<sup>1,2</sup> H. Bideaud,<sup>2</sup> P. Düringer,<sup>3</sup> A. Schröder,<sup>2</sup> C.M. Marques<sup>2</sup>

<sup>1</sup>*Department of Physics & Astronomy, University of Pennsylvania, Philadelphia, PA 19104-6396, USA*

<sup>2</sup>*LDFC-CNRS UMR 7506, 3 rue de l'Université, 67084 Strasbourg Cedex, France and*

<sup>3</sup>*CGS-CNRS UMR 7517, Institut de Géologie, 1 rue Blessig, 67084 Strasbourg Cedex, France*

(Dated: July 16, 2018)

The shapes of flat pebbles may be characterized in terms of the statistical distribution of curvatures measured along their contours. We illustrate this new method for clay pebbles eroded in a controlled laboratory apparatus, and also for naturally-occurring rip-up clasts formed and eroded in the Mont St.-Michel bay. We find that the curvature distribution allows finer discrimination than traditional measures of aspect ratios. Furthermore, it connects to the microscopic action of erosion processes that are typically faster at protruding regions of high curvature. We discuss in detail how the curvature may be reliably deduced from digital photographs.

PACS numbers: 45.70.-n,83.80.Nb,91.60.-x,02.60.Jh

## I. INTRODUCTION

The roundness of pebbles on a beach has long been a source of wonder and astonishment for scientists in many fields [1, 2]. Explanations for the pebble shapes were born from the simple pleasure of understanding nature but also from the hope that a pebble, or a collection of pebbles, might carry lithographically imprinted the signature of their erosion history. Reading that imprint would then, for instance, reveal if a pebble was eroded on a beach, a river or a glacier, or if it traveled a long distance down a stream. It even perhaps would reveal for how long the erosion forces have been at work on that object. Of obvious interest in Geology [3], a physical understanding of the formation of erosion shapes would also allow for a better control of many industrial processes leading to rounded objects such as gem stone or clay bead grinding in tumblers or fruit and vegetable peeling in several mechanical devices. Diverse mathematical tools have been developed for geometrical shape analysis of crystalites, cell membranes, and other far from equilibrium systems [4, 5, 6, 7]; however, these do not seem applicable to pebbles.

The evolution of a pebble shape under erosion can arguably be viewed as a succession of elementary cuts that act at the surface of the body to remove a given amount of material. This converts young, polyhedral-like shapes with a relatively small number of large sides and sharp vertices into more mature shapes with a high number of small sides and smooth vertices. The size and the shapes of each of these successive ablations, as well as the surface sites where the cutting happens, are determined both by the conditions under which erosion takes place and by the nature of the material being eroded. Exposure of a young, polyhedral-like shape to the rough tumbling of a steep stream slope will result in relatively large cuts of the angular sections, while exposure to the gentle erosion of wind or water is more likely to lead to small cuts almost parallel to the existing flat sides. Also, the same sequence of external forces acting on two identical original shapes of different materials will result into distinct

forms due to weight, hardness or anisotropy differences. In spite of the diversity of factors at play in shape modification, the complete evolution of the pebble shape is fully determined by (i) the initial form described by some number of faces, edges and vertices and (ii) the position, size and orientation of the successive ablations.

Given that the erosion process evolves by a succession of localized events on the pebble surface, it is surprising that the majority of the precedent attempts to characterize the pebble shapes were restricted to the determination of global quantities such as the pebble mass or the lengths of its three main axes [3]. Clearly, in order to capture both the local nature of the erosion process and the statistical character of the successive elementary cuts, one needs to build a new detailed description of the pebble shapes based on quantities that are more microscopic and more closely connected to evolution processes. In Ref. [8] we proposed curvature as a key microscopic variable, since, intuitively, protruding regions with large curvature erode faster than flatter regions of small curvature. We then proposed the distribution of curvature around a flat, two-dimensional, pebble as a new statistical tool for shape description. And finally we illustrated and tested these ideas by measuring and modeling the erosion of clay pebbles in a controlled laboratory apparatus.

In this paper we elaborate on our initial Letter [8], and we apply our methods to naturally-occurring rip-up clasts found in the tidal flats of the Mont St.-Michel bay. Section II begins with a survey of shape quantification for two-dimensional objects, in general, and recapitulates our new curvature-based method. Section III provides further details of the laboratory experiments on clay pebbles. Section IV presents a new field study of the Mont St.-Michel rip-up clasts. And finally, following the conclusion, two methods are presented in the Appendix for reliably extracting the local curvature from digital photographs.

## II. 2D SHAPE QUANTIFICATION

The issue of rock shape is of long-standing interest in the field of sedimentology [9, 10, 11, 12, 13, 14, 15, 16, 17]. Two basic methods have become sufficiently well established as to be discussed in introductory textbooks [3]. The simplest is a visual chart for comparing a given rock against a standard sequence of rocks that vary in their sphericity and angularity. A rock has high “*sphericity*” if its three dimensions are nearly equal. And it is “*very angular*”, independent of its sphericity, if the surface has cusps or sharp ridges; the opposite of “very angular” is “*well rounded*”. While useful for exposition, such verbal distinctions are subjective and irreproducible. The second method is to form dimensionless shape indices based on the lengths of three orthogonal axes. From the ratios, and the ratios of differences, of the long to intermediate to short axes, one can readily distinguish rods from discs from spheres. And a given rock may be represented by a point on a triangular diagram according to the values of three such indices, with rod / disc / sphere attained at the corners. This practice is nearly half a century old [18]. Nevertheless, there is still much debate about which of the infinite number of possible shape indices are most useful [19, 20, 21, 22, 23]. In any case, such indices cannot capture fine distinctions in shape, let alone the verbal distinctions of angular vs rounded. Furthermore, they provide no natural connection to the underlying physical process by which the rock was formed.

More recent methods of shape analysis employ Fourier [24, 25, 26, 27], or even wavelet [28], transforms of the contour. This applies naturally to flat pebbles or grains, but also to flat images of three-dimensional objects. The advantage of Fourier analysis over shape indices is that, with enough terms in the series, the exact pebble contour can be reproduced. For simple shapes, the contour may be described in polar coordinates by radius (eg distance from center of mass) vs angle,  $r(\theta)$ , and the corresponding transform. However, this representation is not single-valued for complex shapes with pits or overhangs. Generally, the contour may be described by Cartesian coordinates vs arclength,  $\{x(s), y(s)\}$ , and the corresponding transforms. In any case, the relative amplitudes of different harmonics give an indication of shape in terms of roughness at different length scales. In a different area of science, Fourier representations have proven especially useful for analysis of fluctuations and instabilities of liquid interfaces, membranes, etc. [4, 5, 6]. In practice, for these systems, shape fluctuations are sampled during some time interval and then the average Fourier amplitudes extracted by averaging over many different realizations of the shape. Also, because these phenomena are *linear*, each Fourier component grows or shrinks at some amplitude-independent rate and the evolution is fully determined by a dispersion relation. Unfortunately these features do not hold for the erosion of pebbles. Because each pebble shape only provides one configuration, average quantities need to be built from

a different prescription. Also, there is no *a priori* guaranty that the variables are Gaussian distributed, and one needs a direct space method to better assess the importance of non-linear phenomena. Non-linearity is, we suspect, intrinsically embedded in the erosion mechanisms of pebbles. If one considers for instance a shape represented by a single harmonic in the  $r(\theta)$  representation, it is clear that the peaks will wear more rapidly than the valleys. Therefore the erosion rate cannot be a function of the harmonic number only; it must either be a non-linear function of the amplitude itself or a function coupling many harmonics.

Our aim is to provide an alternative measure of pebble shape that is well-defined, simple, and connects naturally to local properties involved in the evolution process. We restrict our attention to flat pebbles, where an obvious shape index is the aspect ratio of long to short axes. Since erosion processes generally act most strongly on the rough, pointed portions of a rock, we will focus on the local curvature of the pebble contour. Technically, curvature is a vector given by  $\mathbf{K} = d\mathbf{T}/ds$ , the derivative of the unit tangent vector with respect to arclength along the contour [29]. More intuitively, the magnitude of the curvature is the reciprocal of the radius of a circle that mimics the local behavior of the contour. Here we shall adopt the sign convention  $K > 0$  where the contour is convex (as at the tip of a bump) and  $K < 0$  where the contour is concave (as where a chip or bite has been removed from an otherwise round pebble). In the Appendix, we describe two means by which the curvature may be reliably measured at each point along the pebble contour. Note that the average curvature is simply related to the perimeter of the contour:

$$P = 2\pi/\langle K \rangle, \quad (1)$$

which is obviously correct when the shape is a circle.

To describe the shape of a pebble, a very natural quantity is the distribution of curvatures,  $\rho(K)$ , defined such that  $\rho(K)dK$  is the probability that the curvature at some point along the contour lies between  $K$  and  $K+dK$  [8]. In order to distinguish different distributions, as a practical matter, it is more reliable [30] to use the cumulative distribution of curvatures

$$f(K) = \int_0^K \rho(K')dK' \quad (2)$$

Literally,  $f(K)$  is the fraction of the perimeter with curvature *less* than  $K$ . Note that  $f(K)$  increases from 0 to 1 as  $K : 0 \rightarrow \infty$ ; the minimum curvature is where  $f(K)$  first rises above 0, the maximum curvature is where  $f(K)$  first reaches 1, and the median curvature is where  $f(K) = 1/2$ . Unlike for  $\rho(K)$ , it is not necessary to bin the curvature data in order to deduce  $f(K)$ . Instead, just sort the curvature data from smallest to largest and keep a running sum of the arclength segments, normalized by perimeter. Finally, so that the shapes of pebbles of different *sizes* may be compared, it is useful to remove the

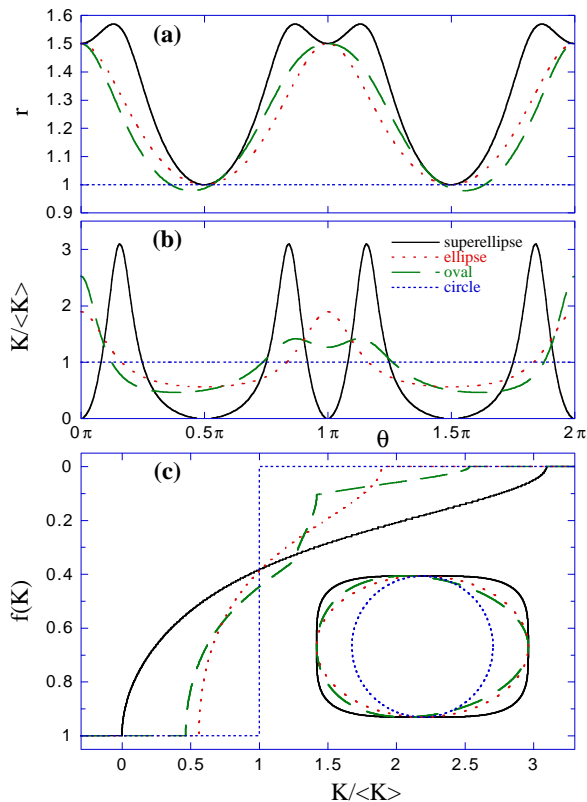


FIG. 1: (a) Radius, (b) normalized curvature and (c) fraction of the perimeter  $f(K)$  with curvature less than  $K$ , vs  $K$  divided by the average curvature  $\langle K \rangle$ , for a superellipse, oval, ellipse, and circle. The curve types match those for the shapes as shown in the inset. Note that, except for the circle, all have the same aspect ratio. The differences in shape are reflected in differences in the forms of  $f(K)$ .

scale factor  $\langle K \rangle$ , which is related to the total perimeter as noted above in Eq. (1). Altogether, we thus propose to quantify pebble shape by examining  $f(K)$  as a function of  $K/\langle K \rangle$ .

To help build intuition, examples of  $f(K)$  are given in Fig. 1 for a few simple shapes. The simplest of all is a circle, where the curvature is the same at each point along the contour:  $K = \langle K \rangle = 2\pi/P = 1/R$ . Thus  $f(K) = 0(1)$  for  $K < (>)\langle K \rangle$ . The curvature distribution is the derivative of this step function, giving  $\rho(K) = \delta(K - \langle K \rangle)$  as required. The other three shapes shown are a superellipse, an oval, and an ellipse. For the latter, with long and short axes  $a$  and  $b$  respectively, one may compute  $f(K) = E(\sin^{-1}[1/\epsilon(1 - (2\sqrt{1 - \epsilon^2}E(\epsilon^2)/(\pi K)^{2/3})^{1/2}], \epsilon^2)/E(\epsilon^2)$  where  $\epsilon = \sqrt{1 - b^2/a^2}$  is the ellipticity,  $E(x)$  is the complete elliptical integral of the first kind and  $E(x, m)$  is the incomplete elliptic integral of the second kind [29].

While noticeably different, the superellipse, ellipse, and oval in Fig. 1 all have the same aspect ratio of 1.5. This emphasizes how a single number is insufficient to quantify shape. The shape differences do, however, show up nicely in the forms of  $f(K)$ . The ellipse is closest to

a circle, with a distribution of curvatures that is most narrowly distributed around the average and hence with an  $f(K)$  that is most like a step function. The superellipse is farthest from a circle, with four long nearly-flat sections and four high-curvature corners; its curvature distribution is broadest. The oval is intermediate.

### III. LABORATORY EXPERIMENT

The examples given in Fig. 1 correspond to regular, highly symmetric shapes of two dimensional convex “pebbles”. In practice, natural or artificial erosion processes lead to curvature functions with an important statistical component. In this section we elaborate on the laboratory experiments of Ref. [8], designed to study both the statistical nature of the curvature distribution and the influence of the original shapes of the pebbles on the final output of a controlled erosion process.

Laboratory pebbles were formed from “chamotte” clay, a kind of clay made from Kaolin and purchased from Graphigro, France. The water content of the purchased clay was 22% in a state that could easily be kneaded. The clay was kept tightly packed before use in order to avoid water evaporation. Clay pebbles were produced using aluminium molds made in our laboratory. They consist of a polygonal well of 0.5 cm depth. Once the mould was filled with clay, it was left at rest for 24 hours, so that 98.5% of the water was removed by evaporation. All the experimental results presented here concern one day old pebbles. We noticed that pebbles older than 2 days were too fragile for our experimental configuration. The dimensions of the various pebbles studied here are as follows: 4 squares of side 5 cm, 5 rectangles of sides  $4 \times 6$  cm<sup>2</sup>, 5 regular pentagons of side 4.25 cm, one triangle with sides 7 cm, 7.5 cm and 9 cm one irregular polygon with 7 sides, one lozenge of acute angles  $45^\circ$  and side 5 cm and one circle of diameter 7 cm.

The wearing method that we chose relies on placing a pebble in the rotating apparatus sketched in Fig. 2. The apparatus is a square basin, of dimensions  $30 \times 30 \times 7$  cm<sup>3</sup>. The basin bottom is a 1 cm thick aluminium plate and the walls are made of 0.04 cm thick aluminium sheets. This rotating plate is fixed to a rod held by the jaws of a laboratory mixer, Heidolph RZR1. The mixer itself is fixed to a tripod, so that its inclination angle can be varied.

A typical trajectory of the pebble during the continuous rotation of the plate can be described as follows. First the pebble rotates with the basin until it reaches a high position. After the plate has rotated an angle between  $\pi/2$  and  $\pi$ , the pebble begins to slide due to gravity, until it hits one of the walls in the bottom part of the container, and then rolls down along that wall as the basin keeps its rotation. After a short stop at a container corner the pebble starts a new cycle again. We performed preliminary tests in order to determine both ideal basin orientation and ideal rotation frequency for



FIG. 2: The wearing apparatus used for the laboratory experiments. The rotating metal tray is  $30 \times 30 \times 7 \text{ cm}^3$ .

our experiments. As expected, above some maximum rotation frequency the pebble becomes immobilised in the basin: centrifugal forces maintain the pebble on a given position against the wall. Also, under some minimum inclination angle, no fall of the pebble is observed, while a high inclination doesn't allow the pebble to reach its maximum altitude. Altogether, we found it suitable to operate at a basin angle of  $45^\circ$  and a rotation frequency of one cycle per second. Using the latter experimental conditions, we observed that the in-plane dimension of a pebble decreased by around a factor 2 after 30 minutes. Thus, a significant wearing of a pebble could be observed after a few minutes rotation. In practice, each pebble was eroded under the described conditions during 30 minutes, while a picture of the pebble was taken after each 5 minutes wearing. Hence, for each of the pebbles studied, we obtained about 7 pictures, corresponding to the initial pebble and to six following states of the wearing pebble. For some of the pebbles 8 or 9 pictures at 5 minutes interval were taken. The images were then analyzed following the method described in the appendix.

An example for the shape evolution produced by this method is given in Fig. 3, with photographs shown every five minutes. The corresponding cumulative curvature distributions  $f(K)$  are given in Fig. 4, where the inset shows the extracted contours. Here the initial shape is square, with four long nearly-flat regions and four short high-curvature regions. Thus the initial  $f(K)$  rises steeply around  $K = 0$  and extends with relatively little weight out to  $K \gg \langle K \rangle$ . At first, the action of ero-

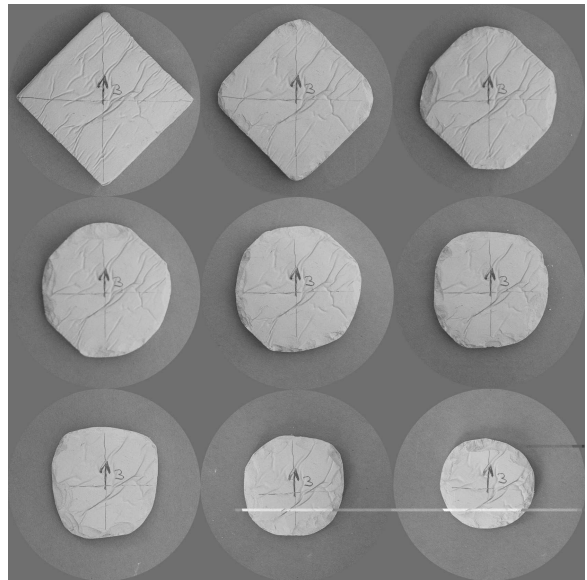


FIG. 3: Shape evolution of a  $5 \times 5 \text{ cm}$  square pebble eroded in the laboratory, by the method explained in the text.

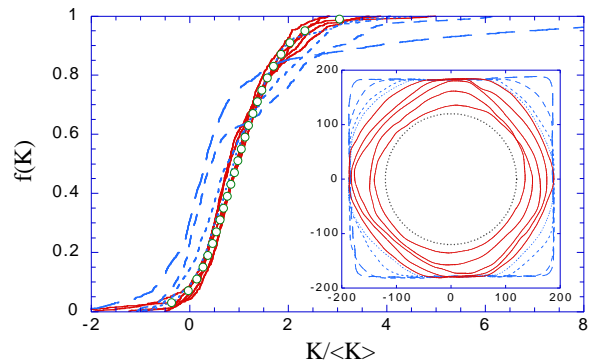


FIG. 4: Cumulative curvature distribution,  $f(K)$ , for the evolving pebble depicted in the inset (and pictured in Fig. 3). As the pebble becomes progressively rounder, the curvature distribution narrows and approaches a final shape. The time interval between successive contours is 5 minutes. For the inset, the axes are given in pixel units, equal to  $0.132 \text{ mm}$ . For contrast, a circle is shown by points.

sion is most rapid at the high-curvature corners, with the flat regions in between relatively unaffected. Thus the high- $K$  tail of  $f(K)$  at first is suppressed, and weight builds up across  $(0.5 - 2)\langle K \rangle$ . Next the rounded corners erode further and gradually extend across the flat sections. Thus weight in  $f(K)$  is gradually concentrated more and more toward  $\langle K \rangle$ . After about 15-20 minutes, when the flat sections are nearly gone, the form of  $f(K)$  fluctuates slightly but ceases to change in any systematic manner. In other words, the shape of the pebble has reached a final limiting form. *Further erosion will affect pebble size, but not pebble shape!*

To test the universality of the final shape, we repeat the same experiment both for other squares as well as for

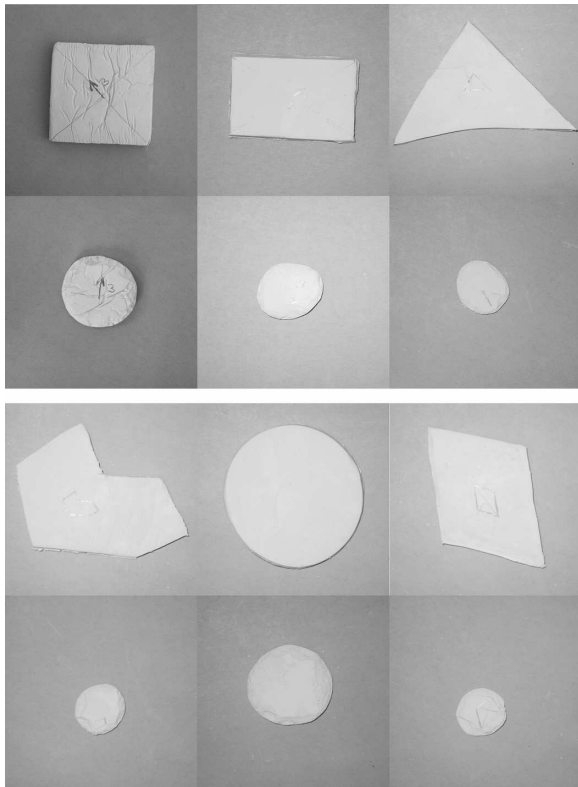


FIG. 5: The initial and final forms of different shapes eroded in our experiment. Final shapes for all cases are not only similar in shape and in size but they have also the same curvature distribution.

a variety of other initial shapes such as rectangles, triangles, and circles. A number of different examples showing both the initial and final shapes are shown in Fig. 5. In all cases, the cumulative curvature distribution  $f(K)$  shows a systematic evolution at short times and slight fluctuations about some average shape at later times, just as in Fig. 4. The more angular or oblong the initial shape, the more erosion is needed to reach a stationary final shape. The average final  $f(K)$  is shown for the various initial shapes in Fig. 6. Evidently, these all display the same quantitative form independent of the initial shape. Even  $f(K)$  for an initially-circular pebble broadens from a step function to the same form as all the others.

The final  $f(K)$  for all initial shapes can thus be averaged together for a more accurate description of the stationary shape produced by the laboratory erosion machine. The result is shown by the open circles in the same plot, Fig. 6. Differentiating, we obtain the actual curvature distribution,  $\rho(K)$ , shown on the right axis. It is fairly broad, with a full-width at half-maximum equal to about  $1.6\langle K \rangle$ . The actual shape is not quite symmetrical, skewed toward higher curvatures. The closest simple analytic form would be a Gaussian,  $\exp[-(K - \langle K \rangle)^2 / (2\sigma^2)]$ . The actual distribution is slightly skewed toward higher curvatures, but the best fit gives a standard deviation of  $\sigma = 0.70\langle K \rangle$ , as shown in Fig. 6. It is easy to imagine

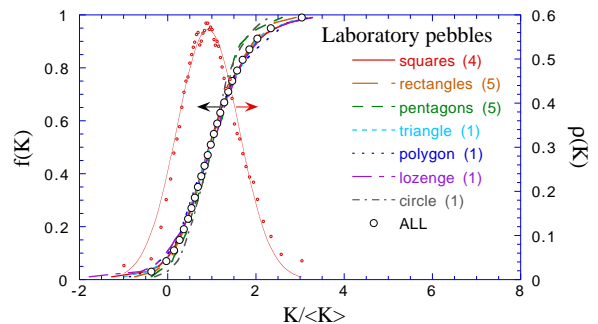


FIG. 6: Integrated curvature distribution,  $f(K)$ , for the final shapes of laboratory pebbles with various initial shapes, as labeled. These are indistinguishable to within measurement accuracy; their average is shown by the open circles. The corresponding average curvature distribution,  $\rho(K)$  is obtained by differentiation and is shown on the right axis along with a fit to a Gaussian shape.

that the width of this distribution could be set by the strength of the erosion process. For example, if the angle of the rotating pan were lowered, then the erosion would be more gradual and more like polishing; in which case a rounder stationary shape may be attained with a narrower distribution of curvatures. The form of  $f(K)$ , as well as its width, could also be affected. These types of questions can be addressed, both in laboratory and field studies, now that we have an incisive tool like  $f(K)$  for quantifying shape.

To further study the erosion produced by our laboratory apparatus, we now consider how the perimeter of the pebble decreases with time,  $P(t)$ . Since the initial behavior depends on the specific initial shape, we focus on subsequent erosion once the (universal) stationary shape is achieved. If the final stationary shape of the curvature distribution is reached at time  $t_0$ , then the quantity of interest is really  $P(t)/P(t_0)$  vs  $t - t_0$ . The results, averaged over all laboratory pebbles, are shown in Fig. 7. Though the dynamic range is not great, the data are consistent with an exponential decrease,  $P(t) = P(t_0) \exp[-(t - t_0)/\tau]$ . The best fit to this form is shown by a solid curve; it gives a decay constant of  $\tau = 44$  min. Exponential erosion is, in fact, observed in field and laboratory studies [12]. It is to be expected whenever the strength of the erosion is proportional to the pebble size, as in our lab experiments where the impulse upon collision is proportional to the pebble's weight.

#### IV. FIELD STUDY

As a first field test of our method of analysis, we collected mud pebbles in the Mont St.-Michel bay, France. The littoral environment located at the inner part of the Norman-Breton Gulf is characterized by a macro-tidal dynamics. This location exhibits the second largest tide

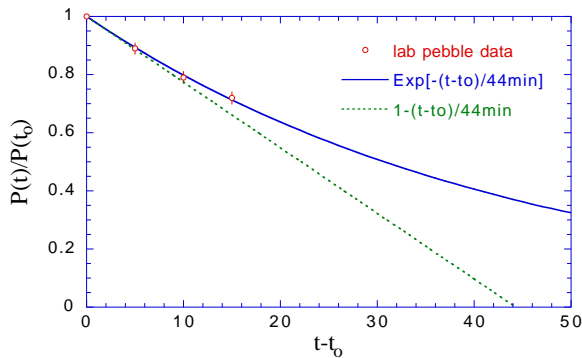


FIG. 7: Perimeter vs time, where  $t_0$  is when the stationary shape has been reached.

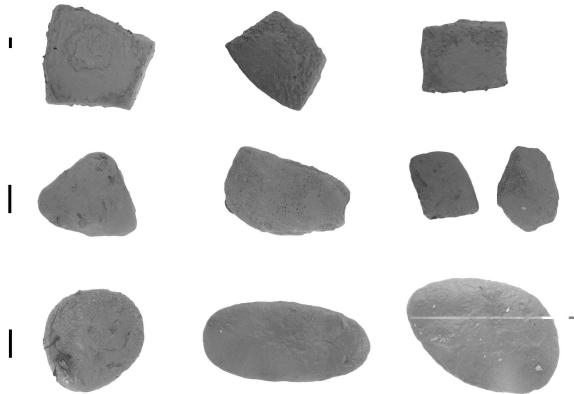


FIG. 8: Typical shapes of Mont St.-Michel rip-up clasts. The immature pebbles in the top row were collected close to their origin; the sub-mature pebbles in the middle row were collected further downstream; the smooth, mature pebbles in the bottom row were collected on a nearby sandbar. As these pebbles eroded, their shapes became rounder, an effect quantified in the next figure. The bars indicate, in each row, a length of 2 cm.

in the world after the Bay of Fundy, Canada. During the spring tide periods the upper part of the tidal flats collects a muddy sediment. This mud dries up during the following neap tide period where the sediments are exposed to the air. In certain areas, between the large equinoctial neap tides, the exposure of mud sediments to air may last for several months. During this period, this mud layer will develop a vast network of desiccation cracks. This network then leads to fragmented plates of a polygonal shape with 20 to 40 cm size. During the next spring tide period, the plates in the erosional area can be eroded by tide currents, thus re-incorporated into the sedimentary cycle. During the tide process these clasts are progressively eroded over many months. Thus the mud cohesion allows enough observation time for the life of a clast to be observed within a distance of order of one hectometer, from the original erosional area down to the latest stages of abrasion.

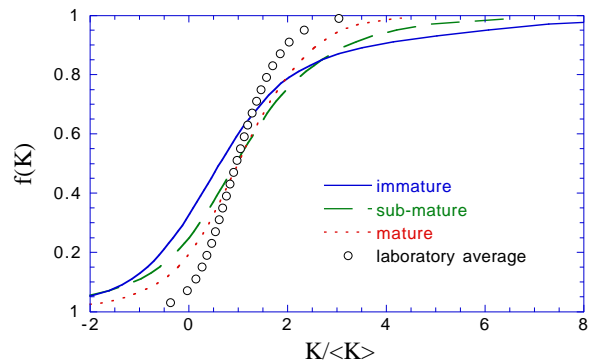


FIG. 9: Cumulative curvature distribution,  $f(K)$ , for the average shapes of Mont St.-Michel rip-up clasts. Even the roundest shapes remained less circular than the final shape in the laboratory study.

We have analyzed the shapes of three classes of rip-up clast photographed at three distinct locations on the tidal flats near Mont St.-Michel. The first is large sub-angular cobble found near the site of formation. Ten samples were examined; for these immature pebbles, the average perimeter is 550 mm. The second class is medium sub-mature pebbles found further “downstream”. As a result of erosion, these pebbles are smaller and smoother than the cobble. Thirty five samples were examined; for these, the average perimeter is 180 mm. The third class is rounded, mature pebbles found on a nearby sand bar. The relation of these pebbles to the other two classes is not clear. Seventeen samples were examined; for these, the average perimeter is 220 mm.

Typical photographs for each of these classes are shown in Fig. 8. The average of the cumulative curvature distribution for all samples in each class is shown in Fig. 9. The angularity of the large cobble is reflected in the breadth of the curvature distribution. Roughly a quarter of the perimeter has negative curvature, and roughly a tenth has curvature five times greater than the average. For the other two classes, the curvature distribution is progressively more narrow. The relative steepness of the  $f(K)$ 's shows that all of these shapes are less round than the final pebbles produced by the laboratory erosion machine.

The width of the curvature distribution can be specified quantitatively by the standard deviation,  $\sigma$ . Results are normalized by the average curvature, and are shown for the field and laboratory pebbles in Table I. The pebbles with steeper  $f(K)$  indeed have smaller widths. For example, the width for the immature field cobble is about 3-4 times that of the average laboratory pebble. While the dimensionless width of the distribution,  $\sigma/\langle K \rangle$ , is a useful number for comparisons, it does not distinguish between curvature distributions of different shape. The actual functional form of the curvature distribution can be specified to some extent by comparing its moments with that of a Gaussian. In particular, the “skewness” and “kurtosis” are dimensionless numbers defined by the

third and fourth moments, respectively, in such a way as to vanish for a perfect Gaussian. The results in Table I show that the four classes of pebbles have curvature distributions of four distinct forms. Of these, the laboratory pebbles are closest to a Gaussian.

Class	Perimeter (mm)	$\sigma/\langle K \rangle$	Skewness	Kurtosis
immature	550±100	2.4±0.3	1.4±0.3	3.8±1.4
sub-mature	180±60	2.0±0.6	0.0±0.9	3.3±2.9
mature	220±70	1.4±0.3	-0.2±0.5	1.3±1.0
lab-final	122±25	0.8±0.1	0.1±0.5	1.0±1.5

TABLE I: Characteristics of curvature distribution for the three classes of field pebbles. Final laboratory pebble shape is added for comparison.

## V. CONCLUSION

We have studied the formation of two-dimensional pebble shapes. As in Ref. [8] we introduced a local description of the erosion process, based on the distribution function of the curvature, measured along the pebble contours. This description captures both the local character of the erosion events, and the statistical nature of the erosion process.

For pebbles generated in the laboratory, we have shown that the curvature distribution has two important properties. First, the erosion drives the distribution towards a stationary form. When this stationary state is reached, the pebble contour still changes but, within small fluctuations, its curvature distribution remains the same, provided that the curvature is normalized by its average value. Secondly, we have found that the final stationary form of the distribution is independent of the original pebble shapes. This not only shows that the curvature distribution is a property of the erosion process itself, but it also opens the interesting possibility of establishing a classification of different erosion processes according to the type of curvature distribution they generate.

For pebbles collected in the field, we have made a first attempt to study a special class of rip-up clasts from the St.-Michel bay. These mud pebbles can be collected at very different erosion stages within a relatively small area of the tidal flats. We showed that the curvature distribution sharpens with the wearing degree, without getting however as sharp as the distribution obtained in the laboratory experiments.

The results presented in this experimental paper suggest a number of directions for modeling the formation of flat pebbles. Of central importance is the intrinsic statistical nature of the erosion process itself. As first hinted in Ref. [8], a sequence of cuts of a noiseless, deterministic nature typically leads to a trivial curvature distribution like that of a circle. We also demonstrated in Ref. [8] that a “cutting” simulation, with an appropriate distribution

of cutting lengths, acting most strongly on regions of high curvature in accord with Aristotle’s intuition [1], can reproduce the curvature distribution from the laboratory experiments. We will address these and other questions relevant for the theoretical modeling of pebble formation in a forthcoming paper.

## Acknowledgments

We acknowledge insightful discussions with F. Thalmann and experimental insight by P. Boltenhagen. This work was supported by the Chemistry Department of the CNRS, under AIP “Soutien aux Jeunes Equipes” (CM). It was also supported by the National Science Foundation under Grant DMR-0514705 (DJD).

## APPENDIX: CURVATURE ANALYSIS

The goal of this section is to provide a detailed, practical description of two means to measure the local curvature at each point along the pebble contour. In both cases the starting point is an image of the pebble. For our work we use a digital camera Canon Power Shot G1 with a resolution of  $1024 \times 768$  pixels. It should be just as effective to scan conventional photographs, or even to scan pebbles themselves. To determine the  $\{x,y\}$  coordinates of the contour, we import the images into NIH Image [31], which includes routines for finding edges and for skeletonizing the result. An example of the digitized pebble contour, and the smooth reconstructions to be discussed below, is given in Fig. 10. We show the contour in pixel units, since the actual calibration is needed only to determine size, not *shape*. Note from the inset that the contour points are indeed pixelized and skeletonized, with each point having only two neighbors located at either  $\pm 1$  or 0 units away in the x- and y-directions. If the digitization process is faithful, then the uncertainty in each pixel is about  $\pm 0.5$  units in each direction. This is not small compared to the distance between neighboring pixels, so a smoothing or fitting routine is necessary to reconstruct the actual contour and thereby extract the curvature distribution.

To illustrate the difficulties of extracting curvature, let us begin with two methods that are, in fact, unsatisfactory. It is perhaps tempting to simply smooth the data, replacing each point with a weighted average of neighbors lying within some window. Weights could be cleverly chosen to de-emphasize points at the edge of the window, for example. This fails, however, since it’s far from obvious how to choose a suitable window size. For instance, the pixelized representation of the straight section given by  $y = 0.1x$  for  $0 < x < 10$  is a step function  $y = 0(1)$  for  $x < (>)5$ . A large window would be needed to even approximately reconstruct the original line. However, such a sufficiently large smoothing window would erase fine features if applied elsewhere along the contour.

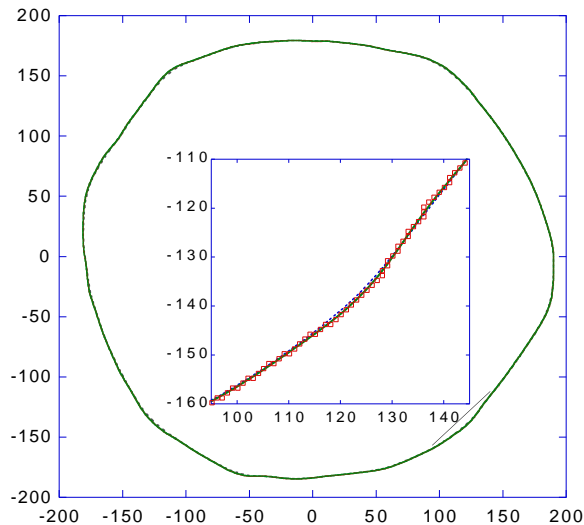


FIG. 10: Reconstruction of a smooth pebble contour from the pixelized digital representation. The solid curve is based on fitting to cubic polynomials at each point. The dashed curve is based on the iteration scheme of Fig. 11.

Since smoothing filters provide no feedback on quality, visual inspection of the result would be necessary to choose an optimal window size at each point along the contour. This is not only subjective, but rather impractical. As an alternative, it is perhaps tempting to implement an automated version of Wentworth’s curvature gauge [9]. This is a device with circular notches of various diameters into which portions of a pebble may be pressed. The computational analogue would be to find the best nonlinear-least-squares fit to a circle at each point along the pebble contour. As with smoothing, one difficulty is to find the optimal window over which to do the fitting. A compounding difficulty is that essentially nowhere is the pebble exactly circular, so even with ‘the’ optimal window there is substantial disagreement between data and fit. A spectacular example of this problem is at an inflection point, where the curvature changes from positive to negative.

To overcome such difficulties, we propose to fit digitized contour data to a cubic polynomial at each point along the contour. A cubic is the lowest order polynomial needed in order to avoid systematic error when the curvature varies gradually across the fitting window, which is the usual case. In order to avoid having to rotate the coordinate system to ensure that the contour  $y(x)$  is a single-valued function, we instead convert to polar coordinates. Thus we define the origin by the center-of-mass of the contour and perform fits to  $r(\theta)$  where  $r = \sqrt{x^2 + y^2}$  and  $\theta = \tan^{-1}(y/x)$ . Once a satisfactory fit is achieved, the curvature may be deduced from the value and derivatives of the cubic polynomial by

$$K = \frac{r^2 + 2r_\theta^2 - rr_{\theta\theta}}{(r^2 + r_\theta^2)^{3/2}}, \quad (\text{A.1})$$

where  $r_\theta = dr/d\theta$  and  $r_{\theta\theta} = d^2r/d\theta^2$  [29].

Two tricks seem necessary to achieve satisfactory results. The first is to weight the data most heavily near the center of the window. We use a Gaussian weighting function with a standard deviation equal to 1/4 of the width of the window. This ensures that points at the edges have essentially no influence. Therefore, the fitting results do not vary rapidly as the window is slid along the contour. This guarantees that the reconstructed curve and its first two derivatives are continuous, which is a crucial requirement for measuring the curvature.

The second trick is to choose the window size appropriately. This is actually the most difficult and subtle aspect of the whole problem. If the window is too small, then the fit will reproduce the bumps and wiggles of the pixelization process; usually the curvature will be overestimated. If the window is too large, then the fit will significantly deviate from the data; usually the curvature will be underestimated. And while the curvature tends to decrease systematically with window size, there is in general, unfortunately, no plateau between these two extremes where the curvature is relatively independent of window size and hence clearly represents the true value. To pick the window appropriately requires careful understanding of the numerical fitting procedure and the feedback it provides. Since the fitting function is a polynomial, the minimization of the  $\chi^2$  total square deviation from the data reduces to solving a set of linear equations. This in turn reduces to inverting a matrix. If the window is too small then the fit will be ‘ambiguous’ in the sense that  $\chi^2$  is small but the error in the fitting parameters is large. Mathematically, the matrix to be inverted is essentially singular. A good strategy is therefore to start with a small window and increase its size until the matrix is no longer singular. This can be accomplished using a linear least-squares fitting routine based on singular-value decomposition [30]. However, the uncertainty in fitting parameters for the first suitable window is generally too large (nearly 100%). So we increase the window size two pixels at a time until the error in curvature has been reduced by a factor of ten. This defines the largest suitable window, beyond which systematic errors due to incorrect functional form begin to appear. We have not been able to define the largest suitable window based on the value of  $\chi^2$ . For the final result, we take a weighted average of the cubic fit parameters over all suitable windows, where the weights are set by the uncertainties in fitting parameters as returned by the fitting routine. An example of a reconstructed contour from this procedure is shown by the solid curve in Fig. 10. The reconstruction is satisfactorily smooth; also, it clearly avoids the pixel noise without smoothing over significant small-scale features in the contour.

Since the cubic fitting method is rather involved, and since the choice of window sizes is still slightly subjective, we have developed an alternative method. The starting point is the fact that the actual digital representation of the contour depends on the location and orientation



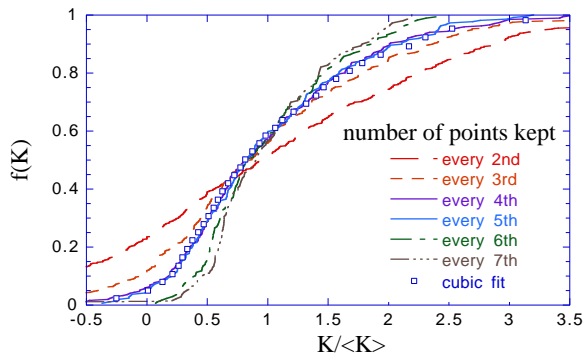


FIG. 11: Trial integrated curvature distributions from the iterative smoothing scheme, vs the number of points kept. Keeping either 4 or 5 points seems optimal: the resulting distributions are identical and they agree with that based on cubic fits.

of the pebble with respect to the grid of pixels. If the pebble were shifted or rotated, then the pixelized representation would be slightly different. For example, imagine the pixelization of a line making various angles with the grid. Perhaps the ideal experimental measurement procedure would be to systematically reposition the pebble, pixelize, then compute the average of all such representations. However this procedure does not lend itself to automatization, and would be impractically time-consuming. Instead, we propose to do more or less the same thing numerically. The idea is to take the current

best guess for the contour, pixelize it with respect to a random grid position and orientation, then use the new representation to update the best guess. When iterated, this procedure converges to a satisfactory reconstruction of the actual contour with two provisos. First, at each step, we locally smooth the trial pixelization by replacing each point by its average with its two immediate neighbors. Second, we keep only every fourth or fifth point in the original pixelized data and perform all operations on this subset. When done, we compute the curvature literally by the change of slope with respect to arclength using the straight segments between adjacent points.

The cumulative curvature distribution given by this iteration scheme is shown in Fig. 11 as a function of the number of points kept. When too many are kept, the reconstructed curve follows the bumps and wiggles of the original pixelization too closely; the curvature distribution is too broad. When too few are kept, the reconstructed curve incorrectly smooths over small-scale features; the curvature distribution is too narrow. When only every fourth or fifth point are kept, the distributions are nearly equal; furthermore, they are indistinguishable from that given by the cubic polynomial fitting. The actual reconstructed contour is also shown in Fig. 10. The plateau in the curvature distribution vs number of points kept, and the good agreement with the other method, both give confidence in this new iterative reconstruction scheme.

- 
- [1] Aristotle, *Minor Works, Mechanical Problems* (Harvard University Press, Cambridge, 2000), translation by W.S. Hett. Question 15 asks: “Why are the stones on the seashore which are called pebbles round, when they are originally made from long stones and shells? Surely it is because in movement what is further from the middle moves more rapidly. For the middle is the center, and the distance from this is the radius. And from an equal movement the greater radius describes a greater circle. But that which travels a greater distance in an equal time describes a greater circle. Things travelling with a greater velocity over a greater distance strike harder, and things which strike harder are themselves struck harder. So that the parts further from the middle must always get worn down. As this happens to them they become round. In the case of pebbles, owing to the movement of the sea and the fact that they are moving with the sea, they are perpetually in motion and are liable to friction as they roll. But this must occur most of all at their extremities.”
- [2] Lord Rayleigh, F.R.S., *Nature* **3901**, 169 (1944).
- [3] S. Boggs, Jr., *Principles of sedimentology and stratigraphy* (Prentice Hall, N.J., 2001), 3rd ed.
- [4] P. M. Chaikin and T. C. Lubensky, *Principles of Condensed Matter Physics* (Cambridge University Press, New York, 1995).
- [5] R. Lipowsky and E. Sackmann, *Structure and dynamics of membranes*, Handbook of biological physics (Elsevier, Amsterdam, 1995).
- [6] P. Meakin, *Fractals, scaling and growth far from equilibrium* (Cambridge University Press, Cambridge, 1998).
- [7] B. Jamtveit and P. Meakin, eds., *Growth, dissolution and pattern formation in geosystems* (Kluwer Academic Publishers, Dordrecht, 1999).
- [8] D. Durian, H. Bideaud, P. Düringer, A. Schroder, F. Thalmann, and C. Marques, *Phys. Rev. Lett* p. to appear (2006).
- [9] C. K. Wentworth, *Journal of Geology* **27**, 507 (1919).
- [10] H. Wadell, *Journal of Geology* **40**, 443 (1932).
- [11] W. C. Krumbein, *Journal of Sedimentary Petrology* **11**, 64 (1941).
- [12] W. C. Krumbein, *Journal of Geology* **49**, 482 (1941).
- [13] A. Cailleux, *C. R. Soc. Geol. Fr. Paris* **13**, 250 (1947).
- [14] G. G. Luttig, *Eizeitaler u. Gegenwart (Ohningen)* **7**, 13 (1956).
- [15] M. Blenk, *Z. Geomorph. Berlin NF 4* **3/4**, 202 (1960).
- [16] P. H. Kuenen, *Geol. Mijnbouw (Leiden)* **44**, 22 (1965).
- [17] P. Düringer, Thèse de doctorat detat, Université Louis Pasteur (1988).
- [18] E. D. Sneed and R. L. Folk, *Journal of Geology* **66**, 114 (1958).
- [19] W. K. Illenberger, *Journal of Sedimentary Petrology* **61**, 756 (1991).
- [20] D. I. Benn and C. K. Ballantyne, *Journal of Sedimentary*

- Petrology **62**, 1147 (1992).
- [21] J. L. Howard, *Sedimentology* **39**, 471 (1992).
- [22] H. J. Hofmann, *Journal of Sedimentology Research* **64**, 916 (1994).
- [23] D. J. Graham and N. G. Midgley, *Earth Surface Processes and Landforms* **25**, 1473 (2000).
- [24] R. Ehrlich and B. Weinberg, *Journal of Sedimentary Petrology* **40**, 205 (1970).
- [25] M. W. Clark, *Journal of the International Association for Mathematical Geology* **13**, 303 (1981).
- [26] M. Diepenbroek, A. Bartholoma, and H. Ibbeken, *Sedimentology* **39**, 411 (1992).
- [27] E. T. Bowman, K. Soga, and W. Drummond, *Geotechnique* **51**, 545 (2001).
- [28] H. Drolon, F. Druaux, and A. Faure, *Pattern Recognition Letters* **21**, 473 (2000).
- [29] E. W. Weisstein, *The CRC concise encyclopedia of mathematics* (CRC Press, New York, 1999).
- [30] W. H. Press, B. P. Flannery, S. A. Teukolsky, and W. T. Vetterling, *Numerical Recipes in C* (Cambridge University Press, New York, 1992), 2nd ed.
- [31] NIH Image, public domain software available at <http://rsb.info.nih.gov/nih-image/>.